

This document contains a post-print version of the paper

Combined Path Following and Compliance Control for Fully Actuated Rigid Body Systems in 3-D Space

authored by **B. Bischof, T. Glück, and A. Kugi**

and published in *IEEE Transactions on Control Systems Technology*.

The content of this post-print version is identical to the published paper but without the publisher's final layout or copy editing. Please, scroll down for the article.

Cite this article as:

B. Bischof, T. Glück, and A. Kugi, "Combined path following and compliance control for fully actuated rigid body systems in 3-d space", *IEEE Transactions on Control Systems Technology*, vol. 25, no. 5, pp. 1750–1760, Sep. 2017, ISSN: 1063-6536. DOI: [10.1109/TCST.2016.2630599](https://doi.org/10.1109/TCST.2016.2630599)

BibTex entry:

```
% This file was created with JabRef 2.8.1.  
% Encoding: Cp1252
```

```
@ARTICLE{acinpaper,  
  author={B. Bischof and T. Gl\"uck and A. Kugi},  
  journal={IEEE Transactions on Control Systems Technology},  
  title={Combined Path Following and Compliance Control for Fully Actuated Rigid Body Systems in 3-D Space},  
  year={2017},  
  volume = {25},  
  number = {5},  
  pages = {1750-1760},  
  doi={10.1109/TCST.2016.2630599},  
  ISSN={1063-6536},  
  month={September}  
}
```

Link to original paper:

<http://dx.doi.org/10.1109/TCST.2016.2630599>

Read more ACIN papers or get this document:

<http://www.acin.tuwien.ac.at/literature>

Contact:

Automation and Control Institute (ACIN)
TU Wien
Gusshausstrasse 27-29/E376
1040 Vienna, Austria

Internet: www.acin.tuwien.ac.at
E-mail: office@acin.tuwien.ac.at
Phone: +43 1 58801 37601
Fax: +43 1 58801 37699

Copyright notice:

© 2017 IEEE. Personal use of this material is permitted. Permission from IEEE must be obtained for all other uses, in any current or future media, including reprinting/republishing this material for advertising or promotional purposes, creating new collective works, for resale or redistribution to servers or lists, or reuse of any copyrighted component of this work in other works.

Combined Path Following and Compliance Control for Fully Actuated Rigid Body Systems in Three-Dimensional Space

Bernhard Bischof, Tobias Glück, and Andreas Kugi, *Member, IEEE*

Abstract—This paper presents path following control for fully actuated rigid body systems in three-dimensional space. Transverse Feedback Linearization and a parallel transport frame are used to design a path following controller that is suitable for paths that are parametrized as regular threefold continuously differentiable curves. The application of this frame enables the handling of paths with zero curvature and reduces the complexity of the control law. The path following controller is combined with a compliance control concept. The strategy is verified by a series of measurement results on a DELTA robot with linear drives.

Index Terms—Path Following Control, Transverse Feedback Linearization, Moving Frame, Compliance Control, Parallel Robot.

I. INTRODUCTION

IN trajectory tracking control, a trajectory which is explicitly parametrized in the time is stabilized. In some tracking control applications, the fixed relationship between the time and the reference is limiting, e.g., when the system cannot be brought to a starting point on the desired trajectory or when the system cannot reach the predefined velocity due to external disturbances or saturation of the plant's input. This limitation can be overcome by path following control (PFC), where the geometry of a desired path, but not the time parametrization, serves as reference.

Early work in the field of the path following problem was done by Samson [1] and Banaszuk [2]. Based on the work of Banaszuk and using input-output feedback linearization, Nielsen and Maggiore introduced the so called Transverse Feedback Linearization (TFL) for input-affine systems in [3]. In TFL, a controlled invariant submanifold of the state space is stabilized. If the system fulfills some sufficient conditions formulated in [3], the dynamics transversal to the submanifold can be linearized via static state feedback. This method was used in [4] to solve the path following problem for a five degrees-of-freedom magnetically levitated positioning system. Reference [5] was concerned with the design of path following controllers for mechanical systems that can be either under- or fully actuated. It was shown that by applying the TFL to fully actuated rigid body systems, the tangential subsystem is linearized as well. However,

B. Bischof and A. Kugi are with the Automation and Control Institute, TU Wien, 1040 Vienna, Austria (e-mail: bischof@acin.tuwien.ac.at, kugi@acin.tuwien.ac.at)

T. Glück is with the Complex Dynamical Systems Department, Austrian Institute of Technology, 1220 Vienna, Austria (e-mail: Tobias.Glueck@ait.ac.at)

the path following controller design method presented in [5] requires both the parametrized and the (closed form) implicit representation of the path. To find a closed form of the implicit representation can be a laborious task or even impossible.

A concept for the design of a path following controller for planar problems using TFL which only depends on the parametrized path representation was proposed in [6]. In this work, an orthonormal frame with respect to a parametrized curve is constructed and the first transversal state is chosen as the projection of the shortest distance to the path onto the normal unit vector.

In three-dimensional Euclidean space, the orthonormal frame with respect to a path is not unique. A common way to construct orthonormal unit vectors is given by the Frenet-Serret frame, see, e.g., [7]. The work [8] extends the path following controller design using the parametric path representation presented in [6] to the three-dimensional Euclidean space. TFL and the Frenet-Serret frame is used to handle paths parametrized by splines.

The Frenet-Serret frame can only be uniquely defined at points on the path where its curvature is nonzero. Moreover the normal vectors become discontinuous when passing points with zero curvature, see, e.g., [7]. In [9], the Frenet-Serret frame was improved by introducing a signed curvature to overcome these drawbacks. However, in a practical application we might be interested in following a path with a curvature close to zero. In this case, the Frenet-Serret frame used in [8] and also the frame proposed in [9] gives rise to extremely high changing rates of the normal vectors leading to a chattering in the control law.

An orthonormal frame with respect to the path, which depends on the idea of relatively parallel fields, was proposed by Bishop in [10]. A normal vector field is said to be relatively parallel along a curve, if its derivative is tangential. This frame, which is often referred to as parallel transport frame [11], is of class C^1 for regular C^2 curves even at points with zero curvature.

In [12] a path following controller for unmanned aerial vehicles (UAVs) is designed. In this work, the position and orientation error to the path is expressed in a parallel

transport frame. An outer nonlinear controller is derived at the kinematic level which solves the path following problem. An inner \mathcal{L}_1 adaptive augmentation loop is designed based on the dynamics of the UAV to improve the overall control performance. Further examples of path following controllers for UAVs using the parallel transport frame are given by [13] and [14]. Note that these approaches are restricted to special vehicle dynamics.

In this paper, we present path following control for fully actuated rigid body systems in three-dimensional space. The presented approach can handle open, closed, and intersecting paths parametrized as regular \mathcal{C}^3 curves. In contrast to [8], the parametrization is split into the position and orientation parametrization and we apply TFL only to the position parametrization to solve the path following control problem. Using a parallel transport frame for the design of the path following controller not only allows to directly cope with paths having zero curvature, it also drastically simplifies the path following control law compared to [8]. Moreover, a feasible neighborhood of the path is defined for which a diffeomorphism can be found that maps the generalized coordinates to tangential, transversal, and rotational coordinates. Following the ideas of [15], where pure planar problems are considered, the method is combined with compliance control. The proposed controller design is applied to a DELTA Robot for a proof of concept. This manipulator, with parallel kinematics, has three translational degrees of freedoms. In a first experiment, a specific motion on a complex path defined by quartic splines in free space is performed. In a second experiment, we demonstrate the combination of the presented path following control strategy with compliance control. To validate the compliant path following control strategy, the end-effector is operated in the notch of a rigid object.

The paper is organized as follows: Section II revisits the rigid body system formulation. Section III is devoted to the path following control strategy. Path assumptions and control objectives are stated in Sections III-A and III-B, respectively. The parallel transport frame is presented in Section III-C and the transformation of the coordinates into the tangential and transversal directions of the path are described in Section III-D. The state feedback law is given in Section III-E and it is shown that the control objectives can be fulfilled. In Section IV, the combination of the path following control with compliance control is described. Section V presents the application of the proposed control strategies to a DELTA robot with linear drives and shows experimental results. A video of a test case is available at http://www.acin.tuwien.ac.at/fileadmin/cds/videos/PFC_and_ComplianceControl_DELTArobot.mp4.

II. MATHEMATICAL MODEL

Let us consider a fully actuated mechanical rigid body system of the form

$$\mathbf{D}(\mathbf{q})\ddot{\mathbf{q}} + \mathbf{n}(\mathbf{q}, \dot{\mathbf{q}}) = \boldsymbol{\tau} + \boldsymbol{\tau}_{ext}, \quad (1a)$$

with

$$\mathbf{n}(\mathbf{q}, \dot{\mathbf{q}}) = \mathbf{C}(\mathbf{q}, \dot{\mathbf{q}})\dot{\mathbf{q}} + \mathbf{g}(\mathbf{q}) + \boldsymbol{\tau}_f(\dot{\mathbf{q}}),$$

generalized configuration coordinates $\mathbf{q} \in \mathbb{R}^m$, generalized forces $\boldsymbol{\tau} \in \mathbb{R}^m$, and external forces/torques $\boldsymbol{\tau}_{ext} \in \mathbb{R}^m$. In (1a), $\mathbf{D}(\mathbf{q}) \in \mathbb{R}^{m \times m}$ denotes the symmetric positive definite generalized mass matrix, $\mathbf{C}(\mathbf{q}, \dot{\mathbf{q}})\dot{\mathbf{q}} \in \mathbb{R}^m$ represents the centrifugal and Coriolis forces, $\mathbf{g}(\mathbf{q}) \in \mathbb{R}^m$ is the vector of potential forces, and friction is modeled by $\boldsymbol{\tau}_f(\dot{\mathbf{q}}) \in \mathbb{R}^m$. The class of outputs \mathbf{y} is restricted to sufficiently smooth functions of the generalized configuration coordinates \mathbf{q} given by

$$\mathbf{y} = \begin{bmatrix} \mathbf{y}_t \\ \mathbf{y}_r \end{bmatrix} = \begin{bmatrix} \mathbf{h}_t(\mathbf{q}) \\ \mathbf{h}_r(\mathbf{q}) \end{bmatrix} = \mathbf{h}(\mathbf{q}), \quad (1b)$$

where $\mathbf{y}_t \in \mathbb{R}^{m_t}$ is the position and $\mathbf{y}_r \in \mathbb{R}^{m_r}$ the orientation in Cartesian coordinates, for instance of the end-effector of a manipulator. In the three-dimensional Euclidean space, $\dim(\mathbf{y}_t) = m_t = 3$ and the orientation, given in some minimal representation, has up to three degrees of freedom, thus, $\dim(\mathbf{y}_r) = m_r \in \{0, 1, 2, 3\}$. Hence, the output dimension is given by $\dim(\mathbf{y}) = m = m_t + m_r \in \{3, 4, 5, 6\}$. For manipulators, \mathbf{y}_t represents the position and \mathbf{y}_r the orientation of an end-effector in a reference frame. In this case, the mappings \mathbf{h} and \mathbf{h}^{-1} are referred to as forward and inverse kinematics, see, e.g., [16]. Note that the first-order time derivative of (1b) results in the differential kinematics equations, see, e.g., [17],

$$\dot{\mathbf{y}} = \begin{bmatrix} \dot{\mathbf{y}}_t \\ \dot{\mathbf{y}}_r \end{bmatrix} = \begin{bmatrix} \nabla \mathbf{h}_t \\ \nabla \mathbf{h}_r \end{bmatrix} \dot{\mathbf{q}} = \mathbf{J}(\mathbf{q})\dot{\mathbf{q}}, \quad (2)$$

with $\nabla \mathbf{h}_t = \partial \mathbf{h}_t / \partial \mathbf{q}$ and $\nabla \mathbf{h}_r = \partial \mathbf{h}_r / \partial \mathbf{q}$, where $\mathbf{J}(\mathbf{q})$ denotes the Jacobian. The second-order time derivative of (1b) yields¹

$$\ddot{\mathbf{y}} = \dot{\mathbf{J}}(\mathbf{q}, \dot{\mathbf{q}})\dot{\mathbf{q}} + \mathbf{J}(\mathbf{q})\ddot{\mathbf{q}}. \quad (3)$$

III. PATH FOLLOWING CONTROL

The objective of path following control is to design a smooth feedback control law that makes the system output approach and move along a path γ where no a priori time parametrization is associated with the movement on the path. The key idea of the presented approach is to find a coordinate transformation, defined in a neighborhood of γ , and a feedback transformation so that the system (1) transforms and linearly decomposes into a tangential $\boldsymbol{\eta}$ -, a transversal $\boldsymbol{\xi}$ -, and a rotational $\boldsymbol{\zeta}$ -subsystem with respect to γ .

A. Path Assumptions

Suppose the path γ is given as a regular \mathcal{C}^3 parametrized curve $\boldsymbol{\sigma}^T(\theta) = [\boldsymbol{\sigma}_t^T(\theta) \quad \boldsymbol{\sigma}_r^T(\theta)] : \mathcal{T} \mapsto \mathbb{R}^m$, with reference position $\boldsymbol{\sigma}_t(\theta) \in \mathbb{R}^{m_t}$, orientation $\boldsymbol{\sigma}_r(\theta) \in \mathbb{R}^{m_r}$, and path parameter θ which is element of a nonempty set $\mathcal{T} \subseteq \mathbb{R}$. For a given parametrization $\boldsymbol{\sigma}(\theta)$, the path γ is defined as $\gamma = \{\bar{\mathbf{y}} \in \mathbb{R}^m : \bar{\mathbf{y}} = \boldsymbol{\sigma}(\bar{\theta}), \bar{\theta} \in \mathcal{T}\}$, where $\boldsymbol{\sigma}_t(\theta)$ defines the position part γ_t and $\boldsymbol{\sigma}_r(\theta)$ the orientation part γ_r . The parametrization $\boldsymbol{\sigma}(\theta)$ of the path γ is regular, if $\boldsymbol{\sigma}'(\bar{\theta}) = (\partial \boldsymbol{\sigma} / \partial \theta)(\bar{\theta}) \neq \mathbf{0}$

¹Note that it is simple to show that $\dot{\mathbf{J}}(\mathbf{q}, \dot{\mathbf{q}})\dot{\mathbf{q}} = \frac{\partial(\mathbf{J}\dot{\mathbf{q}})}{\partial \mathbf{q}}\dot{\mathbf{q}}$ holds.

If θ^* is an interior point of \mathcal{T} , (9) features a strict minimum in a feasible neighborhood, which fulfills the first-order necessary condition for optimality

$$(\mathbf{y}_t - \boldsymbol{\sigma}_t(\theta^*))^T \boldsymbol{\sigma}'_t(\theta^*) = 0 \quad (10)$$

and the second-order sufficient condition for optimality

$$\|\boldsymbol{\sigma}'_t(\theta^*)\|_2^2 - (\mathbf{y}_t - \boldsymbol{\sigma}_t(\theta^*))^T \boldsymbol{\sigma}''_t(\theta^*) > 0, \quad (11)$$

see, e.g., [19]. Because $\boldsymbol{\sigma}'_t(\theta^*)$ is tangential to the path at $\boldsymbol{\sigma}_t(\theta^*)$, (10) implies that the vector $\mathbf{y}_t - \boldsymbol{\sigma}_t(\theta^*)$ is orthogonal to the path, cf. Fig. 1. Rearranging (11) and introducing

$$\alpha(\mathbf{y}_t) = \frac{(\mathbf{y}_t - \boldsymbol{\sigma}_t(\theta^*))^T \boldsymbol{\sigma}''_t(\theta^*)}{\|\boldsymbol{\sigma}'_t(\theta^*)\|_2^2} \quad (12)$$

allows to define the feasible neighborhood of a path $\mathcal{Y}_t = \{\bar{\mathbf{y}}_t \in \mathbb{R}^{m_t} : \alpha(\bar{\mathbf{y}}_t) < 1\}$.

2) *Tangential Subsystem*: The first tangential coordinate is, as proposed in [6], chosen by the arc length

$$\eta_1 = g(\mathbf{y}_t) = \int_{\theta_0}^{\theta^*} \|\boldsymbol{\sigma}'_t(\tau)\|_2 d\tau. \quad (13)$$

See Theorem 1.4.1 in [7] for a definition of the arc length. By differentiating the first-order condition for optimality (10) with respect to the time and using (4) and (12), we obtain the time derivative of the optimal path parameter

$$\dot{\theta}^* = \frac{\beta(\mathbf{y}_t) \mathbf{e}_{||}^T(\theta^*)}{\|\boldsymbol{\sigma}'_t(\theta^*)\|_2} \dot{\mathbf{y}}_t, \quad (14)$$

where

$$\beta(\mathbf{y}_t) = \frac{1}{1 - \alpha(\mathbf{y}_t)}. \quad (15)$$

If the system output is on the path, $\alpha(\mathbf{y}_t = \boldsymbol{\sigma}_t(\theta^*)) = 0$ and $\beta(\mathbf{y}_t = \boldsymbol{\sigma}_t(\theta^*)) = 1$ holds true. Calculating the time derivative of (13) and using (14), the second tangential coordinate follows as

$$\eta_2 = \dot{\eta}_1 = \|\boldsymbol{\sigma}'_t(\theta^*)\|_2 \dot{\theta}^* = \underbrace{\beta(\mathbf{y}_t) \mathbf{e}_{||}^T(\theta^*)}_{(\nabla g)^T} \underbrace{\dot{\mathbf{y}}_t}_{\nabla \mathbf{h}_t \dot{\mathbf{q}}} \quad (16)$$

with gradient $(\nabla g)^T = \partial g / \partial \mathbf{y}_t$ and Jacobian $\nabla \mathbf{h}_t = \partial \mathbf{h}_t / \partial \mathbf{q}$. The limit case $\alpha(\mathbf{y}_t) \rightarrow 1$ implies $\beta(\mathbf{y}_t) \rightarrow \infty$. Hence, small values of $\dot{\mathbf{y}}_t$ result in large derivatives of the arc length. Note that the term $\beta(\mathbf{y}_t)$ is missing in the derivations in [8].

3) *Transversal Subsystem*: The transversal coordinates, ξ_1 and ξ_3 , are defined as the projections of $\mathbf{y}_t - \boldsymbol{\sigma}_t(\theta^*)$ onto the vectors \mathbf{e}_{\perp} and \mathbf{e}_{\parallel} , i.e.,

$$\xi_1 = \delta_1(\mathbf{y}_t) = \mathbf{e}_{\perp}^T(\theta^*) (\mathbf{y}_t - \boldsymbol{\sigma}_t(\theta^*)) \quad (17)$$

and

$$\xi_3 = \delta_2(\mathbf{y}_t) = \mathbf{e}_{\parallel}^T(\theta^*) (\mathbf{y}_t - \boldsymbol{\sigma}_t(\theta^*)). \quad (18)$$

If the output \mathbf{y}_t is on the path, $\xi_1 = \xi_3 = 0$ holds. By differentiating (17) and (18) with respect to the time, we get

$$\begin{aligned} \xi_2 = \dot{\xi}_1 = & \underbrace{(\mathbf{e}'_{\perp}(\theta^*))^T \dot{\theta}^* (\mathbf{y}_t - \boldsymbol{\sigma}_t(\theta^*))}_{\stackrel{(\text{sa})}{=0}} - \underbrace{\mathbf{e}_{\perp}^T(\theta^*) \boldsymbol{\sigma}'_t(\theta^*) \dot{\theta}^*}_{\stackrel{(\text{so})}{=0}} \\ & + \underbrace{\mathbf{e}_{\perp}^T(\theta^*)}_{(\nabla \delta_1)^T} \underbrace{\dot{\mathbf{y}}_t}_{\nabla \mathbf{h}_t \dot{\mathbf{q}}} \end{aligned} \quad (19)$$

and

$$\begin{aligned} \xi_4 = \dot{\xi}_3 = & \underbrace{(\mathbf{e}'_{\parallel}(\theta^*))^T \dot{\theta}^* (\mathbf{y}_t - \boldsymbol{\sigma}_t(\theta^*))}_{\stackrel{(\text{sa})}{=0}} - \underbrace{\mathbf{e}_{\parallel}^T(\theta^*) \boldsymbol{\sigma}'_t(\theta^*) \dot{\theta}^*}_{\stackrel{(\text{so})}{=0}} \\ & + \underbrace{\mathbf{e}_{\parallel}^T(\theta^*)}_{(\nabla \delta_2)^T} \underbrace{\dot{\mathbf{y}}_t}_{\nabla \mathbf{h}_t \dot{\mathbf{q}}} \end{aligned} \quad (20)$$

with gradients $(\nabla \delta_1)^T = \partial \delta_1 / \partial \mathbf{y}_t$ and $(\nabla \delta_2)^T = \partial \delta_2 / \partial \mathbf{y}_t$. Note that the first parts in (19) and (20) are zero due to the usage of the parallel transport frame.

4) *Rotational Subsystem*: The first and second rotational coordinates are chosen as

$$\zeta_1 = \mathbf{y}_r = \mathbf{h}_r(\mathbf{q}) \quad (21)$$

and

$$\zeta_2 = \dot{\zeta}_1 = \dot{\mathbf{y}}_r = \nabla \mathbf{h}_r \dot{\mathbf{q}} \quad (22)$$

with Jacobian $\nabla \mathbf{h}_r = \partial \mathbf{h}_r / \partial \mathbf{q}$.

5) *Diffeomorphism*: The tangential, transversal, and rotational maps, (13) and (16)-(22), are used to construct a \mathcal{C}^1 -diffeomorphism, see, e.g., [20, p.147] for a definition of a diffeomorphism. The virtual output $\hat{\mathbf{y}}^T = \hat{\mathbf{h}}^T(\mathbf{q}) = [\eta_1 \ \xi_1 \ \xi_3 \ \zeta_1^T]^T$ is introduced, which allows us to define the mapping

$$\begin{bmatrix} \hat{\mathbf{y}} \\ \hat{\dot{\mathbf{y}}} \end{bmatrix} = \begin{bmatrix} \eta_1 \\ \xi_1 \\ \xi_3 \\ \zeta_1 \\ \eta_2 \\ \xi_2 \\ \xi_4 \\ \zeta_2 \end{bmatrix} = \begin{bmatrix} g \circ \mathbf{h}_t(\mathbf{q}) \\ \delta_1 \circ \mathbf{h}_t(\mathbf{q}) \\ \delta_2 \circ \mathbf{h}_t(\mathbf{q}) \\ \mathbf{h}_r(\mathbf{q}) \\ (\nabla g)^T \nabla \mathbf{h}_t \dot{\mathbf{q}} \\ (\nabla \delta_1)^T \nabla \mathbf{h}_t \dot{\mathbf{q}} \\ (\nabla \delta_2)^T \nabla \mathbf{h}_t \dot{\mathbf{q}} \\ \nabla \mathbf{h}_r \dot{\mathbf{q}} \end{bmatrix} = \Phi(\mathbf{q}, \dot{\mathbf{q}}). \quad (23)$$

Lemma 1: The mapping $\Phi : \mathcal{X} \mapsto \mathcal{Z}$ with $\mathcal{X} = \mathcal{Q} \times \mathcal{T}_{\mathbf{q}}\mathcal{Q}$, $\mathcal{Q} = \{\bar{\mathbf{q}} \in \mathbb{R}^m : \alpha \circ \mathbf{h}_t(\bar{\mathbf{q}}) < 1\}$, and tangential space $\mathcal{T}_{\mathbf{q}}\mathcal{Q}$ is a \mathcal{C}^1 -diffeomorphism, if $\mathbf{J}(\mathbf{q})$ is nonsingular.

Proof 1: By the inverse function theorem, see, e.g., Theorem 8.2 in [20], we have to show that

- (i.) \mathcal{X} and \mathcal{Z} are open in \mathbb{R}^{2m} ,
- (ii.) $\Phi \in \mathcal{C}^1(\mathcal{X}, \mathcal{Z})$, and
- (iii.) $\nabla \Phi = [\partial \Phi / \partial \mathbf{q} \ \partial \Phi / \partial \dot{\mathbf{q}}]$ is nonsingular for all $[\mathbf{q}^T \ \dot{\mathbf{q}}^T]^T \in \mathcal{X}$.

Since \mathcal{Q} is an open subset of \mathbb{R}^m , \mathcal{X} and \mathcal{Z} are open in \mathbb{R}^{2m} . Since the output $\mathbf{y} = \mathbf{h}(\mathbf{q})$ is assumed to be sufficiently smooth and $\boldsymbol{\sigma}(\theta) \in \mathcal{C}^3(\mathcal{T}, \mathbb{R}^m)$, $\Phi \in \mathcal{C}^1(\mathcal{X}, \mathcal{Z})$ holds. The Jacobian of Φ reads as

$$\nabla \Phi = \begin{bmatrix} \hat{\mathbf{J}}(\mathbf{q}) & \mathbf{0} \\ * & \hat{\mathbf{J}}(\mathbf{q}) \end{bmatrix} \quad (24)$$

with matrices $\hat{\mathbf{J}}(\mathbf{q}) = \mathbf{L}(\mathbf{q})\mathbf{J}(\mathbf{q})$,

$$\mathbf{L}(\mathbf{q}) = \begin{bmatrix} \mathbf{E}(\mathbf{q}) & \mathbf{0} \\ \mathbf{0} & \mathbf{I} \end{bmatrix}, \text{ and } \mathbf{E}(\mathbf{q}) = \begin{bmatrix} \beta(\mathbf{y}_t) \mathbf{e}_{||}^T \\ \mathbf{e}_{\perp}^T \\ \mathbf{e}_{\parallel}^T \end{bmatrix}, \quad (25)$$

where \mathbf{I} is the identity matrix. If $\mathbf{J}(\mathbf{q})$ is nonsingular and $\alpha(\mathbf{y}_t) < 1$, then, $\mathbf{E}(\mathbf{q})$ and $\mathbf{L}(\mathbf{q})$ are nonsingular, $\beta(\mathbf{y}_t) < \infty$, thus, $\nabla \Phi$ is nonsingular for all $[\mathbf{q}^T \ \dot{\mathbf{q}}^T]^T \in \mathcal{X}$.

E. Feedback Transformation

Differentiating the tangential state $\eta_2 = \dot{\eta}_1$ from (16) with respect to the time yields

$$\ddot{\eta}_1 = \left((\nabla\beta)^T \dot{\mathbf{y}}_t \mathbf{e}_{||}^T(\theta^*) + \beta(\mathbf{y}_t) \left(\mathbf{e}'_{||}(\theta^*) \right)^T \dot{\theta}^* \right) \dot{\mathbf{y}}_t + \beta(\mathbf{y}_t) \mathbf{e}_{||}^T(\theta^*) \ddot{\mathbf{y}}_t, \quad (26)$$

where $(\nabla\beta)^T = \partial\beta/\partial\mathbf{y}_t$. The time derivatives of the transversal states $\xi_2 = \dot{\xi}_1$ from (19) and $\xi_4 = \dot{\xi}_3$ from (20) take the form

$$\ddot{\xi}_1 = (\mathbf{e}'_{\perp}(\theta^*))^T \dot{\theta}^* \dot{\mathbf{y}}_t + \mathbf{e}_{\perp}^T(\theta^*) \ddot{\mathbf{y}}_t \quad (27)$$

and

$$\ddot{\xi}_3 = (\mathbf{e}'_{\text{th}}(\theta^*))^T \dot{\theta}^* \dot{\mathbf{y}}_t + \mathbf{e}_{\text{th}}^T(\theta^*) \ddot{\mathbf{y}}_t. \quad (28)$$

The second-order time derivative of ζ_1 from (21) gives

$$\ddot{\zeta}_1 = \ddot{\mathbf{y}}_r. \quad (29)$$

Hence, application of the feedback transformation

$$\boldsymbol{\tau} = \mathbf{n}(\mathbf{q}, \dot{\mathbf{q}}) - \boldsymbol{\tau}_{ext} + \mathbf{D}(\mathbf{q}) \hat{\mathbf{J}}^{-1}(\mathbf{q}) (\mathbf{v} - \dot{\hat{\mathbf{J}}}(\mathbf{q}, \dot{\mathbf{q}}) \dot{\mathbf{q}}) \quad (30)$$

to the system (1), with new control input $\mathbf{v}^T = [\mathbf{v}_t^T \ \mathbf{v}_r^T]$, where $\mathbf{v}_t^T = [v_{||} \ v_{\perp} \ v_{\text{th}}]$ results in a linear input-output relation from the new input \mathbf{v} to the virtual output $\hat{\mathbf{y}}$ in the form of m integrator chains of length two

$$\ddot{\hat{\mathbf{y}}} = \mathbf{v}. \quad (31)$$

Note that the dynamics of the transformed system are linear with respect to a nonlinear plant and a nonlinear path γ . The virtual inputs in the direction of the normal vectors, v_{\perp} and v_{th} , can effectively be used to fulfill objective (O1), i.e., to stabilize the transversal ξ -subsystem and to guarantee asymptotic convergence to $\sigma_t(\cdot)$. The controlled invariant subset is given by $\Gamma^* = \{ [\bar{\mathbf{q}}^T \ \dot{\bar{\mathbf{q}}}^T]^T \in \mathbb{R}^{2m} : \Phi_{\xi}(\bar{\mathbf{q}}, \dot{\bar{\mathbf{q}}}) = \mathbf{0} \}$ with

$$\Phi_{\xi}(\mathbf{q}, \dot{\mathbf{q}}) = \begin{bmatrix} \delta_1 \circ \mathbf{h}_t(\mathbf{q}) \\ \delta_2 \circ \mathbf{h}_t(\mathbf{q}) \\ (\nabla\delta_1)^T \nabla \mathbf{h}_t \dot{\mathbf{q}} \\ (\nabla\delta_2)^T \nabla \mathbf{h}_t \dot{\mathbf{q}} \end{bmatrix}. \quad (32)$$

Thus, objective (O2) is met, because if $[\bar{\mathbf{q}}^T(t_0) \ \dot{\bar{\mathbf{q}}}^T(t_0)]^T \in \Gamma^*$, then, by choosing $v_{\perp} = 0$ and $v_{\text{th}} = 0$, $\xi_i = 0$, with $i = 1, 2, 3, 4$ and $\|\mathbf{y}_t(t)\|_{\gamma_t} = 0 \ \forall t > t_0$. Moreover, the virtual input in tangential direction $v_{||}$ allows to control the motion along the path, thus, objective (O3) can be satisfied.

IV. COMBINED PATH FOLLOWING AND COMPLIANCE CONTROL

Compliance control addresses a classical problem in robotics of simultaneously controlling the position and the interaction forces with the environment. In the following, it is shown how to combine the presented path following control concept with compliance control. For this, a position-based impedance control is employed, see [21]. In position-based impedance control, the compliance is realized by tracking

the trajectory of the exponentially stable reference impedance model using position control in an inner control loop and an impedance control in the outer loop. As shown in [22], this method is well suited for accurate positioning in free space as well as in contact with rigid environments. Due to the possibility of using high gains in the inner loop, the position-based impedance control is rather insensitive to model uncertainties.

A. Compliance Control

The fundamental idea of compliance control is to design a controller which imposes a reference dynamics (impedance) between external forces and the position. In our case, the reference impedance of the motion along and orthogonal to the path γ_t as well as the reference impedance of the orientation can be separately defined as

$$\begin{bmatrix} \tau_{||} \\ \tau_{\perp} \\ \tau_{\text{th}} \\ \tau_r \end{bmatrix} = \begin{bmatrix} m_{||}^d \ddot{e}_{\eta}^d + d_{||}^d \dot{e}_{\eta}^d + k_{||}^d e_{\eta}^d \\ m_{\perp}^d \ddot{\xi}_1 + d_{\perp}^d \dot{\xi}_1 + k_{\perp}^d \xi_1 \\ m_{\text{th}}^d \ddot{\xi}_3 + d_{\text{th}}^d \dot{\xi}_3 + k_{\text{th}}^d \xi_3 \\ m_r^d \ddot{\mathbf{e}}_r^d + d_r^d \dot{\mathbf{e}}_r^d + k_r^d \mathbf{e}_r^d \end{bmatrix}, \quad (33)$$

where $e_{\eta}^d = \eta_1 - \eta_1^d$ denotes the error between the tangential coordinate η_1 and a reference η_1^d and $\mathbf{e}_r^d = \mathbf{y}_r - \boldsymbol{\sigma}_r(\theta^*)$. Moreover, m_i^d , d_i^d and k_i^d for $i = \{||, \perp, r\}$ are constant design parameters and

$$\begin{bmatrix} \tau_{||} \\ \tau_{\perp} \\ \tau_{\text{th}} \\ \tau_r \end{bmatrix} = \hat{\mathbf{J}}^{-T} \boldsymbol{\tau}_{ext} = \begin{bmatrix} \frac{1}{\beta} \mathbf{e}_{||}^T & \mathbf{0} \\ \mathbf{e}_{\perp}^T & \mathbf{0} \\ \mathbf{e}_{\text{th}}^T & \mathbf{0} \\ \mathbf{0} & \mathbf{I} \end{bmatrix} \mathbf{J}^{-T} \boldsymbol{\tau}_{ext} \quad (34)$$

are the external (projected) generalized forces.

B. Compliant Transverse Feedback Linearization

Assuming perfect tracking of the inner position loop, the actual tangential and transversal coordinates η_1 , ξ_1 , and ξ_3 as well as the orientation \mathbf{y}_r can be replaced by the references η_1^p , ξ_1^p , ξ_3^p , and \mathbf{y}_r^p in (33). Introducing the errors $e_{\eta}^{pd} = \eta_1^p - \eta_1^d$ and $\mathbf{e}_r^{pd} = \mathbf{y}_r^p - \boldsymbol{\sigma}_r(\theta^*)$ allows us to deduce the impedance control law

$$\ddot{\eta}_1^p = \ddot{\eta}_1^d + \frac{\tau_{||}}{m_{||}^d} - \frac{d_{||}^d}{m_{||}^d} \dot{e}_{\eta}^{pd} - \frac{k_{||}^d}{m_{||}^d} e_{\eta}^{pd}, \quad (35a)$$

$$\dot{\eta}_1^p = \int_0^t \ddot{\eta}_1^p d\tau, \quad \eta_1^p = \int_0^t \dot{\eta}_1^p d\tau,$$

$$\ddot{\xi}_1^p = \frac{\tau_{\perp}}{m_{\perp}^d} - \frac{d_{\perp}^d}{m_{\perp}^d} \dot{\xi}_1^p - \frac{k_{\perp}^d}{m_{\perp}^d} \xi_1^p, \quad (35b)$$

$$\dot{\xi}_1^p = \int_0^t \ddot{\xi}_1^p d\tau, \quad \xi_1^p = \int_0^t \dot{\xi}_1^p d\tau,$$

$$\ddot{\xi}_3^p = \frac{\tau_{\text{th}}}{m_{\text{th}}^d} - \frac{d_{\text{th}}^d}{m_{\text{th}}^d} \dot{\xi}_3^p - \frac{k_{\text{th}}^d}{m_{\text{th}}^d} \xi_3^p, \quad (35c)$$

$$\dot{\xi}_3^p = \int_0^t \ddot{\xi}_3^p d\tau, \quad \xi_3^p = \int_0^t \dot{\xi}_3^p d\tau,$$

$$\ddot{\mathbf{y}}_r^p = \ddot{\boldsymbol{\sigma}}_r(\theta^*) + \frac{\boldsymbol{\tau}_r}{m_r^d} - \frac{d_r^d}{m_r^d} \dot{\mathbf{e}}_r^{pd} - \frac{k_r^d}{m_r^d} \mathbf{e}_r^{pd},$$

$$\dot{\mathbf{y}}_r^p = \int_0^t \ddot{\mathbf{y}}_r^p d\tau, \quad \mathbf{y}_r^p = \int_0^t \dot{\mathbf{y}}_r^p d\tau.$$
(35d)

In the inner position control loop, the feedback transformation (30) and the control law

$$\mathbf{v} = \begin{bmatrix} \mathbf{v}_t \\ \mathbf{v}_r \end{bmatrix} = \begin{bmatrix} \ddot{\eta}_1^p - a_{\eta,2} \dot{e}_\eta^p - a_{\eta,1} e_\eta^p \\ \ddot{\xi}_1^p - a_{\xi,2} \dot{e}_\xi^p - a_{\xi,1} e_\xi^p \\ \ddot{\xi}_3^p - a_{\xi,2} \dot{e}_\xi^p - a_{\xi,1} e_\xi^p \\ \ddot{\mathbf{y}}_r^p - a_{r,2} \dot{\mathbf{e}}_r^p - a_{r,1} \mathbf{e}_r^p \end{bmatrix}$$
(36)

is used, where $e_\eta^p = \eta_1 - \eta_1^p$, $e_{\xi_i}^p = \xi_i - \xi_i^p$, and $\mathbf{e}_r^p = \mathbf{y}_r - \mathbf{y}_r^p$. The control law (36) yields exponentially stable error dynamics, if $a_{i,j} > 0$ with $i \in \{\eta, \xi, r\}$ and $j = 1, 2$.

In the case of $\mathbf{y}_r \in \mathbb{R}^3$ the definitions of $\dot{\mathbf{y}}_r^p$ in (35d) and \mathbf{v}_r in (36) suffer from representation singularities and the rotational stiffness depends on the reference orientation $\boldsymbol{\sigma}_r(\theta^*)$, see [23]. Methods to avoid these disadvantages are shown in [23], e.g. the local orientation error representation. They can also be used for the control concept presented in this section.

V. APPLICATION TO A DELTA ROBOT

The presented path following controller is applied to a linear drive, parallel kinematic, DELTA robot of the type FESTO EXPT-45, which is shown in Fig. 2.

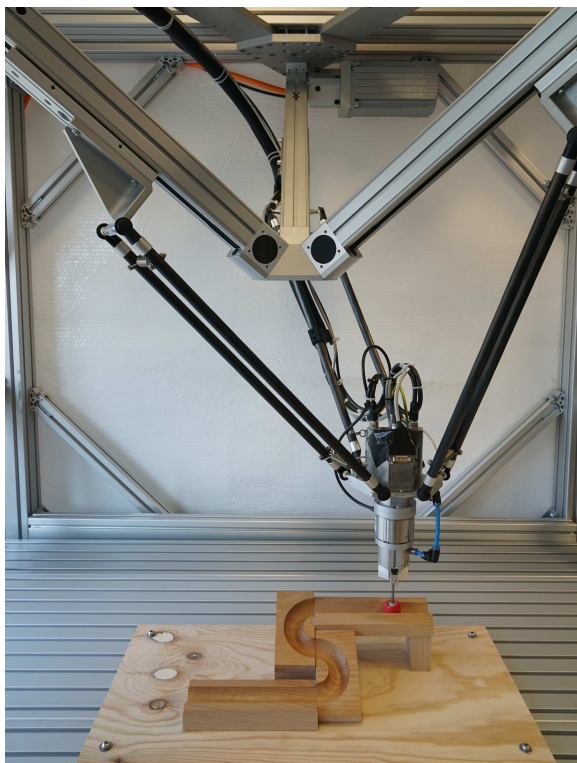


Fig. 2. DELTA Robot FESTO EXPT-45.

A. Mathematical Model

The mathematical modeling of DELTA robots with three translational degrees of freedom was presented in [24] and its kinematics and dynamics are discussed in literature, see, e.g., [25], [26], [27], [28], and [29]. In these works, DELTA robots with rotary drives are considered. For the DELTA robot FESTO EXPT-45 with linear drives the kinematics and dynamics are quite similar. Fig. 3 shows a schematic diagram

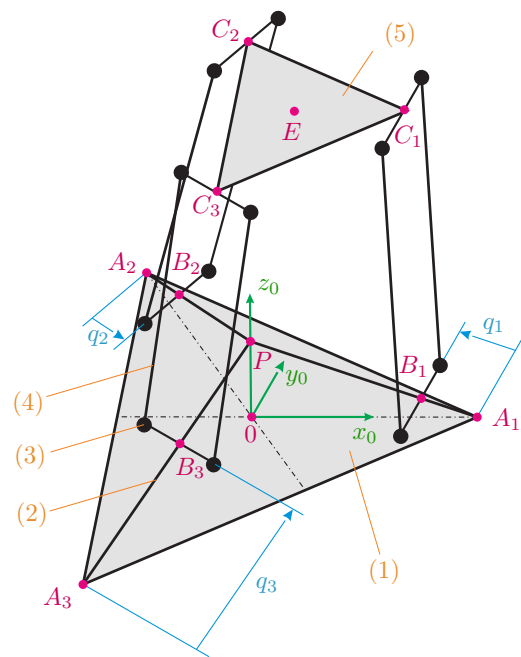


Fig. 3. Schematic diagram of a DELTA robot with linear drives.

of the considered DELTA robot with linear drives. The DELTA robot has three translational and no rotational degrees of freedom, i.e., $m_r = 0$ and $m = m_t = 3$. The robot basically consists of a base plate (1), the end-effector plate (5), three parallelogram arms (4), and three electric linear drives (2). The linear drives are symmetrically arranged. They are mounted at the points A_i , $i = 1, 2, 3$, at the base plate and at a joint point P . The three parallelogram arms are fixed to the slides of the linear drives at B_i , $i = 1, 2, 3$, and the end-effector plate at the points C_i , $i = 1, 2, 3$. The rods of the parallelogram (4) are on both sides attached via ball joints (3). The inertial coordinate system is given by $(0, x_0, y_0, z_0)$ with the center of area of the base plate 0 as origin and the x_0 -axis pointing from 0 to A_1 . The position of the slides B_i with respect to A_i along the segment $\overline{A_i P}$ serve as generalized coordinates q_i , $i = 1, 2, 3$. Hence, the vector of generalized coordinates reads as $\mathbf{q}^T = [q_1 \ q_2 \ q_3]$. The system output $\mathbf{y}^T = [y_x \ y_y \ y_z]$ is defined as the vector, expressed in the inertial coordinate system, from the origin 0 to E , which is fixed to the end-effector plate.

The DELTA robot with linear drives features unique and smooth solutions for the forward and inverse kinematics $\mathbf{y} = \mathbf{h}(\mathbf{q})$ and $\mathbf{q} = \mathbf{h}^{-1}(\mathbf{y})$, respectively. The system dynamics can be expressed in the form (1), where the generalized forces $\boldsymbol{\tau}^T = \boldsymbol{\tau}_q^T = [\tau_{q,1} \ \tau_{q,2} \ \tau_{q,3}]$ are the linear drive forces and $\boldsymbol{\tau}_y^T = [\tau_{y,1} \ \tau_{y,2} \ \tau_{y,3}] = (\mathbf{J}^{-T} \boldsymbol{\tau}_{ext})^T$ are the external end-effector forces.

B. Implementation

The proposed static state feedback controller is implemented on the real-time system DS1006 from DSPACE with a sampling time of $T_s = 1$ ms. A time discretization in the form $t = kT_s, k = 1, 2, \dots$ is performed. For the time-discrete implementation of (30), the optimization problem (9), the integral (13), and the differential-algebraic equations (5) have to be numerically solved in real time.

1) *Numerical Solution of the Optimization Problem and Integration:* The optimization problem (9) is numerically solved using the Newton method. For the initialization, the global optimum θ_0^* is needed. A sufficient number of evenly spread points on the path γ_t are chosen and the distances to $\mathbf{y}_t(0)$ are calculated. The point with shortest distance is used as starting point for the local minimum search to obtain θ_0^* . Then, the optimization problem (9) is iteratively solved in each time step $k = 1, 2, \dots$ for $i = 1, 2, \dots$ according to

$$\theta_{k,i} = \theta_{k,i-1} - \frac{J'(\theta_{k,i-1})}{J''(\theta_{k,i-1})}, \quad (37)$$

with initial condition $\theta_{k,0} = \theta_{k-1}^*$ and cost function $J(\theta_{k,i-1}) = \|\mathbf{y}_{t,k} - \boldsymbol{\sigma}_t(\theta_{k,i-1})\|_2^2$ until $|\theta_{k,i} - \theta_{k,i-1}| < \varepsilon$. The optimal solution $\theta_k^* = \theta_{k,i}$ is used to perform the numerical integration of (13), i.e.,

$$\eta_{1,k} = \eta_{1,k-1} + (\theta_k^* - \theta_{k-1}^*) \|\boldsymbol{\sigma}'_t(\theta_k^*)\|_2, \quad (38)$$

where $\eta_{1,k} = \eta_1(kT_s)$.

2) *Discretization of the Parallel Transport Frame:* A discrete method to calculate the normal vectors of the parallel transport frame is proposed in [11]. In every time step $k = 1, 2, \dots$ a rotation axis and an angle is determined from the tangential vectors $\mathbf{e}_{||,k}$ and $\mathbf{e}_{||,k-1}$ and the normal vectors are rotated with respect to them. The approach is ill-conditioned for small changes of the tangential vectors. Hence, we present another approach that solves directly the overdetermined problem (5) to find the first normal vector $\mathbf{e}_\perp(\theta)$. Application of the constant step-size backward Euler method, see, e.g., [18], to (5) for $i = \perp$ yields

$$\begin{aligned} \mathbf{e}_{\perp,k} &= \mathbf{e}_{\perp,k-1} + T_s \gamma_{\perp,k} \mathbf{e}_{||,k} \\ 0 &= 1 - \mathbf{e}_{\perp,k}^T \mathbf{e}_{\perp,k} \\ 0 &= \mathbf{e}_{||,k}^T \mathbf{e}_{\perp,k}, \end{aligned} \quad (39)$$

where $\mathbf{e}_{\perp,k} = \mathbf{e}_\perp(kT_s)$. The overdetermined equations (39) have no solution for $T_s > 0$. A straightforward idea is to

search for a least-squares solution of (39), see [18]. Therefore, the constrained least-squares problem

$$\begin{aligned} \min_{\mathbf{p}_k \in \mathbb{R}^4} f(\mathbf{p}_k) &= \frac{1}{2} \|\mathbf{e}_{\perp,k-1} - \mathbf{e}_{\perp,k} + T_s \gamma_{\perp,k} \mathbf{e}_{||,k}\|_2^2 \\ \text{s.t. } g_1(\mathbf{p}_k) &= \frac{1}{2} (\mathbf{e}_{\perp,k}^T \mathbf{e}_{\perp,k} - 1) = 0 \\ g_2(\mathbf{p}_k) &= \mathbf{e}_{||,k}^T \mathbf{e}_{\perp,k} = 0, \end{aligned} \quad (40)$$

with $\mathbf{p}_k = [\mathbf{e}_{\perp,k}^T \ \gamma_{\perp,k}]^T$ and fixed k , is considered. The optimal solution $\mathbf{p}_k^* = [(\mathbf{e}_{\perp,k}^*)^T \ \gamma_{\perp,k}^*]^T$ of (40) is found using the first-order optimality condition of (40), i.e.,

$$(\nabla f)(\mathbf{p}_k^*) + \lambda_1^* (\nabla g_1)(\mathbf{p}_k^*) + \lambda_2^* (\nabla g_2)(\mathbf{p}_k^*) = \mathbf{0} \quad (41a)$$

$$g_1(\mathbf{p}_k^*) = 0 \quad (41b)$$

$$g_2(\mathbf{p}_k^*) = 0, \quad (41c)$$

with Lagrange multipliers λ_1^* and λ_2^* and gradients

$$\begin{aligned} (\nabla f)^T &= \frac{\partial f}{\partial \mathbf{p}_k} = \left[-(\mathbf{e}_{\perp,k-1}^* - \mathbf{e}_{\perp,k}^* + T_s \gamma_{\perp,k}^* \mathbf{e}_{||,k}^*)^T, \right. \\ &\quad \left. T_s (\mathbf{e}_{\perp,k-1}^* - \mathbf{e}_{\perp,k}^* + T_s \gamma_{\perp,k}^* \mathbf{e}_{||,k}^*)^T \mathbf{e}_{||,k}^* \right] \\ (\nabla g_1)^T &= \frac{\partial g_1}{\partial \mathbf{p}_k} = \left[(\mathbf{e}_{\perp,k}^*)^T \ 0 \right] \\ (\nabla g_2)^T &= \frac{\partial g_2}{\partial \mathbf{p}_k} = \left[\mathbf{e}_{||,k}^T \ 0 \right]. \end{aligned} \quad (42)$$

From the last row of (41a) and (41c), we obtain

$$\gamma_{\perp,k}^* = -\frac{1}{T_s} \mathbf{e}_{||,k}^T \mathbf{e}_{\perp,k-1}^*. \quad (43)$$

Multiplying (41a) by $\mathbf{e}_{||,k}^T$ and using (41b) and (41c) yields $\lambda_2^* = 0$ and

$$\mathbf{e}_{\perp,k}^* = \frac{1}{1 + \lambda_1^*} (\mathbf{e}_{\perp,k-1}^* - \mathbf{e}_{||,k}^T \mathbf{e}_{\perp,k-1}^* \mathbf{e}_{||,k}^*). \quad (44)$$

Inserting (44) into (41c) results in

$$1 + \lambda_1^* = \pm \sqrt{1 - (\mathbf{e}_{||,k}^T \mathbf{e}_{\perp,k-1}^*)^2}. \quad (45)$$

Thus, (40) features the analytic solution

$$\mathbf{e}_{\perp,k}^* = \frac{\mathbf{e}_{\perp,k-1}^* - \mathbf{e}_{||,k}^T \mathbf{e}_{\perp,k-1}^* \mathbf{e}_{||,k}^*}{\sqrt{1 - (\mathbf{e}_{||,k}^T \mathbf{e}_{\perp,k-1}^*)^2}}, \quad (46)$$

which represents an iteration for the first normal vector $\mathbf{e}_{\perp,k}$.

Remark 1: To ensure continuity of $\mathbf{e}_{\perp,k}^*$ the positive solution of (45) has to be used.

The iteration (46), without derivation, can also be found in [30]. Note that the initial condition for the iteration (46), i.e., $\mathbf{e}_\perp(\theta_0) = \mathbf{e}_{\perp,1}$, must comply with the algebraic equations of (39). In Appendix A, it is shown that the iteration (46) converges to the solution of (7) for $T_s \rightarrow 0$. The second normal vector $\mathbf{e}_{\perp 2}(\theta)$ is calculated using (8).

C. Path Parametrization

To demonstrate the path following control approach, quartic splines are used, which are of class C^3 , to represent a path γ . In particular, a parametrization $\sigma(\theta) : \mathcal{T} \mapsto \mathbb{R}^m$ of the form

$$\sigma(\theta) = \begin{cases} \sigma_0(\theta), & \theta_0 \leq \theta < \theta_1 \\ \sigma_1(\theta), & \theta_1 \leq \theta < \theta_2 \\ \vdots \\ \sigma_{l-1}(\theta), & \theta_{l-1} \leq \theta \leq \theta_l \end{cases} \quad (47a)$$

consisting of l path segments with

$$\sigma_s(\theta) = \sigma|_{[\theta_s, \theta_{s+1})}(\theta) = \sum_{j=0}^4 \begin{bmatrix} a_{j,s}(\theta - \theta_s)^j \\ b_{j,s}(\theta - \theta_s)^j \\ c_{j,s}(\theta - \theta_s)^j \end{bmatrix} \quad (47b)$$

and suitable coefficients $a_{j,s}$, $b_{j,s}$, $c_{j,s}$, $j = 0, \dots, 4$ and $s = 0, \dots, l-1$ is considered.

D. Path Following Control of the DELTA Robot

Choosing the virtual output $\hat{\mathbf{y}}^T = \hat{\mathbf{h}}^T(\mathbf{q}) = [\eta_1 \ \xi_1 \ \xi_3]$ according to (13), (17) and (18) and applying the feedback transformation (30) results in

$$\ddot{\hat{\mathbf{y}}} = \begin{bmatrix} \ddot{\eta}_1 \\ \ddot{\xi}_1 \\ \ddot{\xi}_3 \end{bmatrix} = \begin{bmatrix} v_{||} \\ v_{\perp} \\ v_{\phi} \end{bmatrix} = \mathbf{v}. \quad (48)$$

The position controller

$$\mathbf{v} = \begin{bmatrix} \ddot{\eta}_1^p - a_{\eta,2}\dot{e}_{\eta}^p - a_{\eta,1}e_{\eta}^p - a_{\eta,0} \int_0^t e_{\eta}^p d\tau \\ \ddot{\xi}_1^p - a_{\xi,2}\dot{e}_{\xi_1}^p - a_{\xi,1}e_{\xi_1}^p - a_{\xi,0} \int_0^t e_{\xi_1}^p d\tau \\ \ddot{\xi}_3^p - a_{\xi,2}\dot{e}_{\xi_3}^p - a_{\xi,1}e_{\xi_3}^p - a_{\xi,0} \int_0^t e_{\xi_3}^p d\tau \end{bmatrix} \quad (49)$$

with references η_1^p , ξ_1^p , and ξ_3^p , yields an exponentially stable linear closed-loop error dynamics which can be arbitrarily assigned by suitable constant parameters $a_{i,j} > 0$ for $i \in \{\eta, \xi\}$ and $j = 0, 1, 2$. In position control, the references in transversal direction, ξ_1^p and ξ_3^p , and their derivatives are usually set to zero.

For the first experiment, a teach-in procedure followed by a quartic spline interpolation was performed, cf. (47). The resulting path γ is depicted in Fig. 4.

A reference η_1^p for the tangential coordinate η_1 is generated which smoothly connects the starting point $\eta_{1,0}^p = 0.022$ m and the end point $\eta_{1,T}^p = 0.31$ m with a maximum velocity of $\eta_{2,\max} = 0.1$ m/s. The references in transversal direction, ξ_1^p and ξ_3^p , and their derivatives are set to zero, cf. (49). The controller parameters are shown in Table I. The end-

TABLE I
CONTROLLER PARAMETERS.

Symbol	Value	Unit	Symbol	Value	Unit
$a_{\eta,0}$	42875	1/s ³	$a_{\xi,0}$	125000	1/s ³
$a_{\eta,1}$	3675	1/s ²	$a_{\xi,1}$	7500	1/s ²
$a_{\eta,2}$	105	1/s	$a_{\xi,2}$	150	1/s

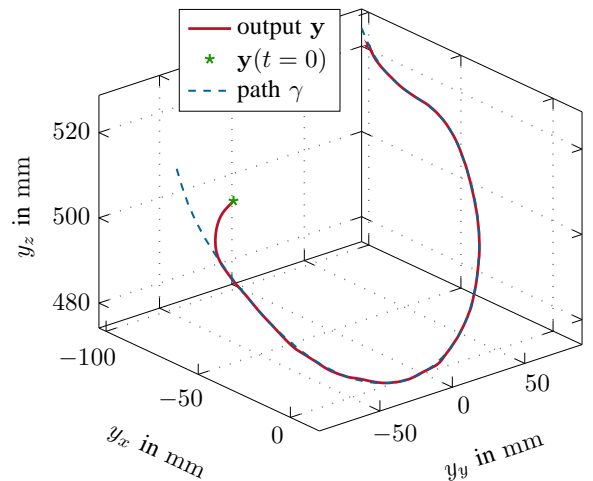


Fig. 4. Path γ and measured output \mathbf{y} .

effector was initially placed next to the path. Fig. 4 depicts the measured output \mathbf{y} which obviously converges to the path γ . Fig. 5 on the left in the first row shows the tangential coordinate η_1 and the reference η_1^p . The measurements clearly show that control objective (O3), defined in Section II, is fulfilled. The transversal states ξ_1 and ξ_3 , depicted in the second row, quickly converge to zero and stay approximately at zero, hence, the control objectives (O1) and (O2) are also satisfied. The deviation of the transversal states from zero is mainly caused by the sticking friction in the linear drives. The last row shows in addition the virtual control input $\mathbf{v}^T = [v_{||} \ v_{\perp} \ v_{\phi}]$. In the right column, the time evolutions of the generalized coordinates, velocities, and forces are shown.

E. Compliant Path Following Control of the DELTA Robot

To illustrate the compliant path following control strategy, the end-effector of the robot is operated in a notch. This is a typical task which may occur in automatic glue dispersion, where the environment is not exactly known. Fig. 2 shows the tripod, a ball with a soft shell, which is fixed to the robot via a gripper, and a ball notch. A teach-in procedure is performed and the path γ is recorded and interpolated using quartic splines, see Section V-C. The task of this experiment is to move the end-effector with the ball along a ball notch from $\eta_{1,0}^d = 0.02$ m to $\eta_{1,T}^d = 0.49$ m with a maximum velocity of $\eta_{2,\max}^d = 0.5$ m/s. If the recorded path exactly conforms with the real path this task is not a problem at all. However, if the workpiece with the ball notch is displaced with respect to the recorded path, the end-effector with the ball gets in contact with the environment. Pure position control would either damage the ball notch of the workpiece, break the end-effector or harm the ball joints of the DELTA robot.

In the considered experiment, the workpiece is displaced -2.5 mm in x -direction and 5.5 mm in y -direction. The feedback transformation (30), the control law (49), and the impedance control law (35), with the control parameters from

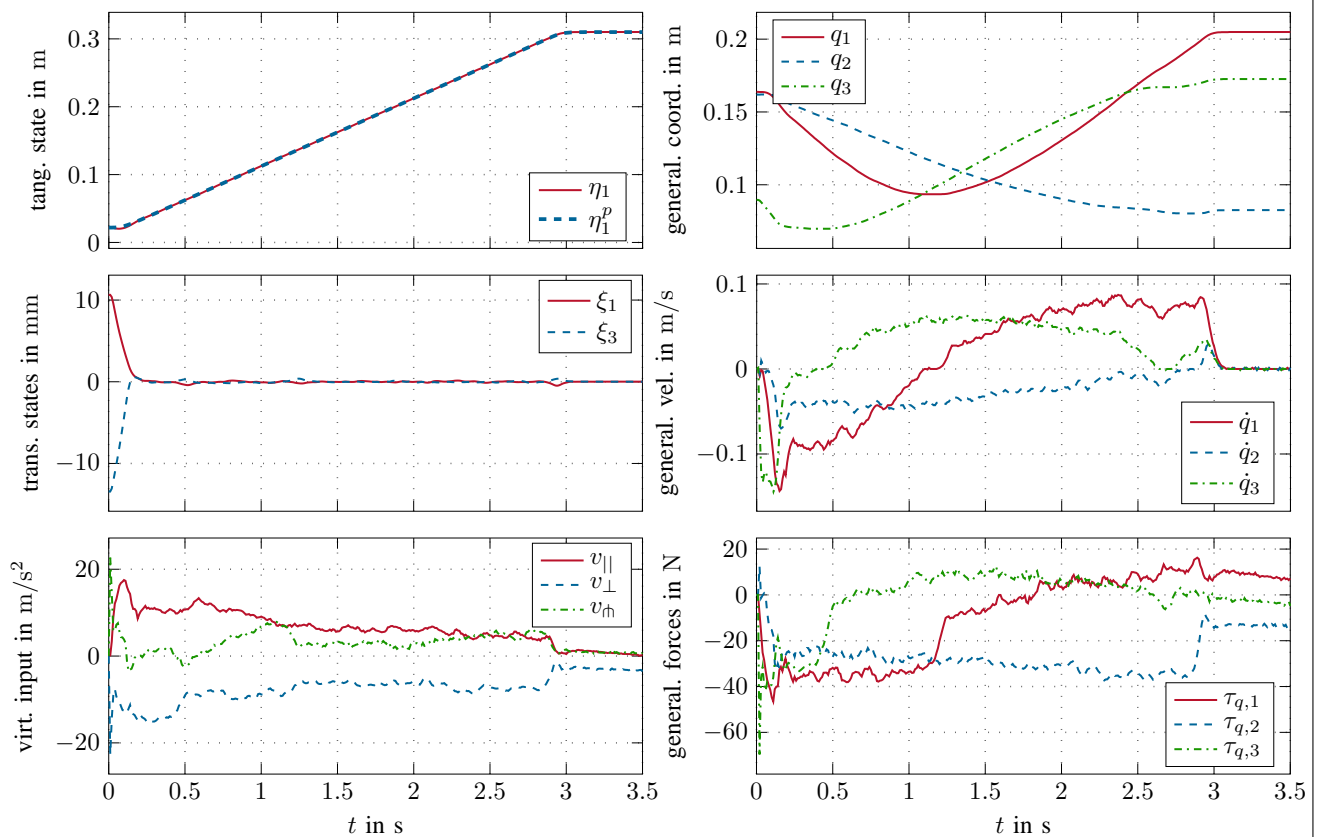


Fig. 5. Experimental results of the path following control strategy.

Tables I and II, are executed on the DSPACE system with a sampling time of $T_s = 1$ ms. The damping ratio of the virtual spring-damper-mass systems is defined as $\zeta^d = 5$, which results in the damping constants $d_i^d = 2\zeta^d \sqrt{m_i^d k_i^d}$, for $i \in \{\parallel, \perp\}$. This relatively high damping is required to ensure contact stability, see, e.g., [31] for more information. To measure the external force τ_y , the six-axis force sensor K6 – D40 from ME-MESSYSTEME is used. Fig. 6 shows

TABLE II
COMPLIANCE CONTROL PARAMETERS.

Symbol	Value	Unit	Symbol	Value	Unit
m_{\parallel}^d	0.3	kg	m_{\perp}^d	0.3	kg
d_{\parallel}^d	300	Ns/m	d_{\perp}^d	122.47	Ns/m
k_{\parallel}^d	3	kN/m	k_{\perp}^d	0.5	kN/m

that the output y deviates from the original path γ due to the displacement of the workpiece with the ball notch. However, the proposed control strategy is still able to move the ball with maximum velocity inside the notch. As shown in Fig. 7 on the left hand side, the reference motion η_1^p along the path can be tracked very well. The position errors in the transversal states are smaller than 1 mm. Note that the characteristics of ξ_1^p and ξ_3^p correspond to the displacement of the notch. The forces acting on the ball during the movement are depicted in Fig. 7

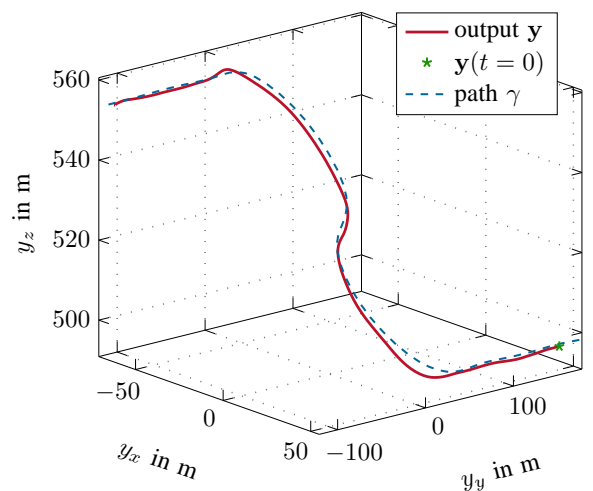


Fig. 6. Path γ and measured output y with compliance control.

on the right hand side. The force in tangential direction τ_{\parallel} is mainly caused by friction between the ball and the notch. In addition, the inputs τ_q , i.e. the forces of the linear drives, are shown.

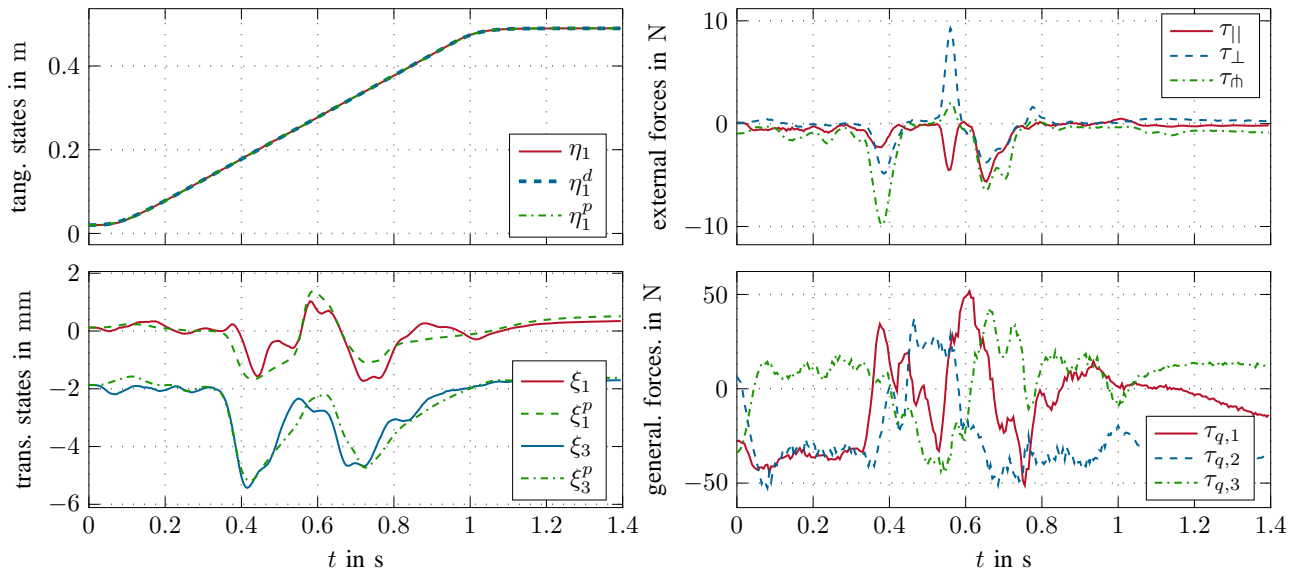


Fig. 7. Experimental results of the compliant path following control strategy.

VI. CONCLUSION

This paper presents path following control for fully actuated rigid body systems in three-dimensional space. The proposed path following control strategy is suitable for any path that can be parametrized as a regular C^3 curve, e.g., using quartic splines. Application of the parallel transport frame not only allows us to handle paths with zero curvature but also simplifies the path following control law compared to e.g. the Frenet-Serret frame. Additionally, due to the structure of the proposed path following control concept, we are able to combine this strategy with compliance control with respect to the path. For experimental validation the proposed controller is applied to a DELTA robot. These experiments include standard path following control in free space as well as the combination with compliance control. Although the DELTA robot has only three translational degrees of freedom, the proposed method is formulated for up to six degrees of freedom and can easily be applied to a 6-axis industrial robot.

APPENDIX A

In the following, we prove that the iteration (46) converges to the solution of (5) for $T_s \rightarrow 0$. The difference equation (46) reads as

$$\mathbf{e}_{\perp,k} \sqrt{1 - (\mathbf{e}_{\perp,k-1}^T \mathbf{e}_{\parallel,k})^2} - \mathbf{e}_{\perp,k-1} = -\mathbf{e}_{\perp,k-1}^T \mathbf{e}_{\parallel,k} \mathbf{e}_{\parallel,k}. \quad (50)$$

Substitution of (43) on the left hand side in (50), dividing by T_s , and taking the limit results in

$$\begin{aligned} & \lim_{T_s \rightarrow 0} \frac{\sqrt{1 - T_s^2 \gamma_{\perp,k}^2} \mathbf{e}_{\perp,k} - \mathbf{e}_{\perp,k-1}}{T_s} \\ &= \dot{\mathbf{e}}_{\perp} + \lim_{T_s \rightarrow 0} \frac{\sqrt{1 - T_s^2 \gamma_{\perp,k}^2} - 1}{T_s} \mathbf{e}_{\perp,k} = \dot{\mathbf{e}}_{\perp} = \mathbf{e}'_{\perp} \dot{\theta}. \end{aligned} \quad (51)$$

By inserting (41c) for $k - 1$ on the right hand side in (50), dividing by T_s , and taking the limit, we get

$$-\lim_{T_s \rightarrow 0} \mathbf{e}_{\perp,k-1}^T \frac{\mathbf{e}_{\parallel,k} - \mathbf{e}_{\parallel,k-1}}{T_s} \mathbf{e}_{\parallel,k} = -\mathbf{e}_{\perp}^T \dot{\mathbf{e}}_{\parallel} \mathbf{e}_{\parallel} = -\mathbf{e}_{\perp}^T \mathbf{e}'_{\parallel} \dot{\theta}. \quad (52)$$

Thus, in the limit case $T_s \rightarrow 0$, the iteration (46) resembles (7) and the iteration (46) numerically solves the differential-algebraic system (5).

REFERENCES

- [1] C. Samson, "Path following and time-varying feedback stabilization of a wheeled mobile robot," in *Proceedings of the International Conference on Automation, Robotics and Computer Vision (ICARCV) 1992*, Singapore, September 1992, pp. RO-13.1.1?RO-13.1.5.
- [2] A. Banaszuk and J. Hauser, "Feedback linearization of transverse dynamics for periodic orbits," in *Proceedings of the 33rd IEEE Conference on Decision and Control 1994*, vol. 2, Lake Buena Vista, Florida, USA, December 1994, pp. 1639-1644.
- [3] C. Nielsen and M. Maggiore, "On local transverse feedback linearization," *SIAM Journal on Control and Optimization*, vol. 47, no. 5, pp. 2227-2250, 2008.
- [4] C. Nielsen and D. Wang, "Path following using transverse feedback linearization: Application to a maglev positioning system," in *Proceedings of the American Control Conference*, St. Louis, MO, USA, June 2009, pp. 3045-3050.
- [5] A. Hladio, C. Nielsen, and D. Wang, "Path following for a class of mechanical systems," *IEEE Transactions on Control Systems Technology*, vol. 21, no. 6, pp. 2380-2390, Nov 2013.
- [6] L. Consolini, M. Maggiore, C. Nielsen, and M. Tosques, "Path following for the pvtol aircraft," *Automatica*, vol. 46, pp. 1284-1296, 2010.
- [7] V. A. Toponogov, *Differential Geometry of Curves and Surfaces*. Boston: Birkhaeuser, 2006.
- [8] R. Gill, D. Kulić, and C. Nielsen, "Spline path following for redundant mechanical systems," *IEEE Transaction on Robotics*, vol. 31, no. 6, pp. 1378-1392, 2015.
- [9] D. Carrol, E. Köse, and I. Sterling, "Improving frenet's frame using bishop's frame," *Journal of Mathematics Research*, vol. 5, no. 4, pp. 97-106, 2013.
- [10] R. L. Bishop, "There is more than one way to frame a curve," *American Mathematical Monthly*, vol. 82, no. 3, pp. 246-251, 1975.
- [11] A. J. Hanson, *Visualizing Quaternions*. San Francisco, USA: Morgan Kaufmann, 2006.

- [12] I. Kaminer, A. Pascoal, E. Xargay, N. Hovakimyan, C. Cao, and V. Dobrokhodov, "Path following for small unmanned aerial vehicles using \mathcal{L}_1 adaptive augmentation of commercial autopilots," *Journal of Guidance, Control and Dynamics*, vol. 33, pp. 550–564, 2010.
- [13] V. Cichella, R. Naldi, V. Dobrokhodov, I. Kaminer, and L. Marconi, "On 3d path following control of a ducted-fan uav on so(3)," in *Decision and Control and European Control Conference (CDC-ECC), 2011 50th IEEE Conference on*, Orlando, Florida, USA, Dec 2011, pp. 3578–3583.
- [14] T. Oliveira, P. Encarnacao, and A. Aguiar, "Moving path following for autonomous robotic vehicles," in *Control Conference (ECC), 2013 European*, Zurich, Switzerland, July 2013, pp. 3320–3325.
- [15] S. Flixeder, T. Glueck, M. Boeck, and A. Kugi, "Combined path following and compliance control with application to a biaxial gantry robot," in *Proceedings of the 2014 IEEE Conference on Control Applications (CCA)*, Antibes, France, October 2014, pp. 796–801.
- [16] R. M. Murray, Z. Li, and S. S. Sastry, *Robotic Manipulation*. Boca Raton, FL: CRC Press, 1994.
- [17] B. Siciliano, L. Sciavicco, L. Villani, and G. Oriolo, *Robotics: Modelling, Planning and Control*. London: Springer, 2009.
- [18] E. Hairer and G. Wanner, *Solving Ordinary Differential Equations II: Stiff and Differential-Algebraic Problems*, 2nd ed. Berlin Heidelberg: Springer, 2010.
- [19] D. Luenberger and Y. Ye, *Linear and Nonlinear Programming*, 3rd ed. New-York: Springer, 2008.
- [20] J. R. Munkres, *Analysis on Manifolds*. Redwood City: Addison-Wesley, 1993.
- [21] W.-S. Lu and Q.-H. Meng, "Impedance control with adaptation for robotic manipulators," *IEEE Transactions on Robotics and Automation*, vol. 7, no. 3, pp. 408–415, June 1991.
- [22] S. Chiaverini, B. Siciliano, and L. Villani, "A survey of robot interaction control schemes with experimental comparison," *IEEE Transactions on Mechatronics*, vol. 4, no. 3, pp. 273–285, Sept 1999.
- [23] F. Caccavale, C. Natale, B. Siciliano, and L. Villani, "Six-dof impedance control based on angle/axis representations," *IEEE Transactions on Robotics and Automation*, vol. 15, no. 2, pp. 289–300, April 1999.
- [24] R. Clavel, "Delta, a fast robot with parallel geometry," in *Proceedings of the 18th International Symposium on Industrial Robots (ISIR)*, Lausanne, Switzerland, April 1988, pp. 91–100.
- [25] —, "Conception d'un robot parallèle rapide à 4 degrés de liberté," Ph.D. dissertation, Swiss Federal Institute of Technology Lausanne (EPFL), 1991.
- [26] A. Codourey, "Contribution à la commande des robots rapides et précis. application au robot delta à entraînement direct," Ph.D. dissertation, Swiss Federal Institute of Technology Lausanne (EPFL), 1991.
- [27] —, "Dynamic modelling and mass matrix evaluation of the delta parallel robot for axes decoupling control," in *Proceedings of the 1996 IEEE/RSJ International Conference on Intelligent Robots and Systems, IROS 96*, vol. 3, Osaka, Japan, November 1996, pp. 1211–1218.
- [28] P. Guglielmetti, "Model-based control of fast parallel robots," Ph.D. dissertation, Swiss Federal Institute of Technology Lausanne (EPFL), 1994.
- [29] K. Miller and R. Clavel, "The lagrange-based model of delta-4 robot dynamics," *Robotersysteme*, vol. 8, pp. 49–54, 1992.
- [30] H. Ma, "Curve and surface framing for scientific visualization and domain dependent navigation," Ph.D. dissertation, Indiana University, Department of Computer Science, Bloomington, Indiana, USA, 1996.
- [31] D. Surdilović, "Contact stability issues in position based impedance control: Theory and experiments," in *Proceedings of the 1996 IEEE International Conference on Robotics and Automation*, vol. 2, Minnesota, USA, April 1996, pp. 1675–1680.



Tobias Glück received the diploma in engineering cybernetics from the University of Stuttgart, Stuttgart, Germany, in 2007, and the Ph.D. (Dr.techn.) degree in electrical engineering from TU Wien, Vienna, Austria, in 2013. He is currently with the Austrian Institute of Technology, Vienna, Austria. His current research interests include physics-based modeling and control of mechatronic systems.



Andreas Kugi (M'94) received the Dipl.-Ing. degree in electrical engineering from Graz University of Technology, Austria, and the Ph.D. degree in control engineering from Johannes Kepler University (JKU), Linz, Austria, in 1992 and 1995, respectively. He received his Habilitation degree in the field of automatic control and control theory from JKU in 2000.

From 1995 to 2000 he worked as an assistant professor and from 2000 to 2002 as an associate professor at JKU. In 2002, he was appointed full professor at Saarland University, Saarbrücken, Germany, where he held the Chair of System Theory and Automatic Control until May 2007. Since June 2007 he is a full professor for complex dynamical systems and head of the Automation and Control Institute at Vienna University of Technology (TU Wien), Austria. His research interests include the physics-based mathematical modeling and control of (nonlinear) mechatronic systems, differential geometric and algebraic methods for nonlinear control, model predictive control and the controller design for infinite-dimensional systems. He is full member of the Austrian Academy of Sciences and Editor-in-Chief of the *Control Engineering Practice*.



Bernhard Bischof received the Dipl.-Ing.(FH) degree in electronics from the UAS Technikum Wien, Vienna, Austria, in 2003.

He has been a research assistant with the Automation and Control Institute, TU Wien, Vienna, since 2014. His current research interests include physics-based mathematical modeling and control of mechatronic systems.